Scientific Research Publishing

Open Journal of Geology, 2024, 14, 629-653
https://www.scirp.org/journal/ojg
ISSN Online: 2161-7589
ISSN Print: 2161-7570

Petrology of Spinel-Lherzolite Xenoliths from Mazélé and Others Northen Xenoliths Localities of Cameroon Volcanic Line: Exchange Reactions and Equilibrium State

Nguihdama Dagwai[1*], Kamgang Pierre[2], Mbowou Gbambié Isaac Bertrand[3], Chazot Gilles[4], Ngounouno Ismaïla[3]

[1]Department of Life and Earth Sciences, Higher Teachers' Training College, University of Maroua, Maroua, Cameroon
[2]Department of Earth Sciences, Faculty of Science, University of Yaoundé 1, Yaoundé, Cameroon
[3]Department of Mineral Prospecting and Exploration Technologies, School of Geology and Mining Engineering, University of Ngaoundere, Meiganga, Cameroon
[4]Ocean Geosciences Laboratory, European University Institute of the Sea (IUEM), Brest, France
Email: *da_nguihdama76@yahoo.fr

How to cite this paper: Dagwai, N., Pierre, K., Bertrand, M.G.I., Gilles, C. and Ismaïla, N. (2024) Petrology of Spinel-Lherzolite Xenoliths from Mazélé and Others Northen Xenoliths Localities of Cameroon Volcanic Line: Exchange Reactions and Equilibrium State. *Open Journal of Geology*, **14**, 629-653.
https://doi.org/10.4236/ojg.2024.145027

Received: April 25, 2024
Accepted: May 26, 2024
Published: May 29, 2024

Abstract

The alkaline volcanism of the Cameroon Volcanic Line in its northern domain has raised many fresh enclaves of peridotites. The samples selected come from five (05) different localities (Liri, in the plateau of Kapsiki, Mazélé in the NE of Ngaoundéré, Tello and Ganguiré in the SE of Ngaoundéré and Likok, locality located in the west of Ngaoundé). The peridotite enclaves of the above localities show restricted mineralogical variation. Most are four-phase spinel-lherzolites, indicating that this is the main lithology that forms the lithospheric mantle below the shallow zone. No traces of garnet or primary plagioclase were detected, which strongly limits the depth range from which the rock fragments were sampled. The textures and the wide equilibrium temperatures (884˚C - 1115˚C) indicate also entrainment of lherzolite xenoliths from shallow depths within the lithosphere and the presence of mantle diapirism. The exchange reactions and equilibrium state established in this work make it possible to characterize the chemical composition of the upper mantle of each region and test the equilibrium state of the phases between them. Variations of major oxides and incompatible elemental concentrations in clinopyroxene indicate a primary control by partial melting. The absence of typical "metasomatic" minerals, low equilibration temperatures and enriched LREE patterns indicate that the upper mantle below septentrional crust of Cameroun underwent an event of cryptic metasomatic enrichment prior to partial melting. The distinctive chemical features, LREE

enrichment, strong U, Ce and Pr, depletion relative to Ba, Nb, La, Pb, and T, fractionation of Zr and Hf and therefore ligh high Zr/Hf ratio, low La/Yb, Nb/La and Ti/Eu are all results of interaction of refractory peridotite residues with carbonatite melts.

Keywords

Xenoliths, Upper Mantle, Northern Region, Adamawa, Cameroon Volcanic Line, Exchange Reaction

1. Introduction

The "Cameroon Volcanic Line" (LVC) is an active tectono-magmatic alignment oriented N30˚E, from the island of Pagalù to Lake Chad, [1] **Figure 1**. This line is a major geological structure in Central Africa whose importance can be compared to the "Rift-Valley system" of East Africa [2]. This chain of intraplate volcanoes covers more than 1600 km long [3] and 100 km wide.

Several scientific researches have been the subject of study both on the geophysical and geological level in the continental part of the Volcanic Line of Cameroon. We recall that according to the authors, geophysical studies have made it possible to better understand the composition, the constitution of its subsoil and its internal structure. In addition, we note that the study of ultramafic xenoliths in general and spinel lherzolites in particular makes it possible to determine the state of stress, pressure and temperature which reign above the upper mantle of this part. The tectonic phenomena which reigned in this part will undoubtedly bring about a slight modification in the lithological composition. Gravity data characterized by a negative anomaly of maximum amplitude 120 mgals [4]-[9] have made it possible to characterize the Adamaoua horst in the Ngaoundéré region. The seismological study [10] reveals a propagation of relatively slow wave speeds (waves P = 7.8 km/s) at the level of Adamaoua indicating the presence of an abnormal upper mantle. It is generally accepted that the "uplift" zones come from the isostatic response linked to a thinning of the lithosphere, itself due to a crustal extension [11]. The crust is thin (about 23 km) and the P-wave velocity in the upper mantle is slow (about 7.8 km/s) compared to the southern part of the plateau where normal values are observed (about 33 km and 8 km/s respectively). The tectonic model according to which the uplift of the Adamaoua would be a thermal bulge resulting from the thinning of the lithosphere and the crust does not on its own explain the results obtained which highlight a significant asymmetry [12]. In recent years, mantle metasomatism has been invoked to account for the geochemical and isotopic inhomogeneities within the upper mantle documented in peridotite xenoliths entrained in kimberlite and alkali basalts. Although metasomatism in the xenoliths is partly attributed to the transporting magma, most metasomatism takes place before entrainment and is of interest, particularly if its effect can be correlated

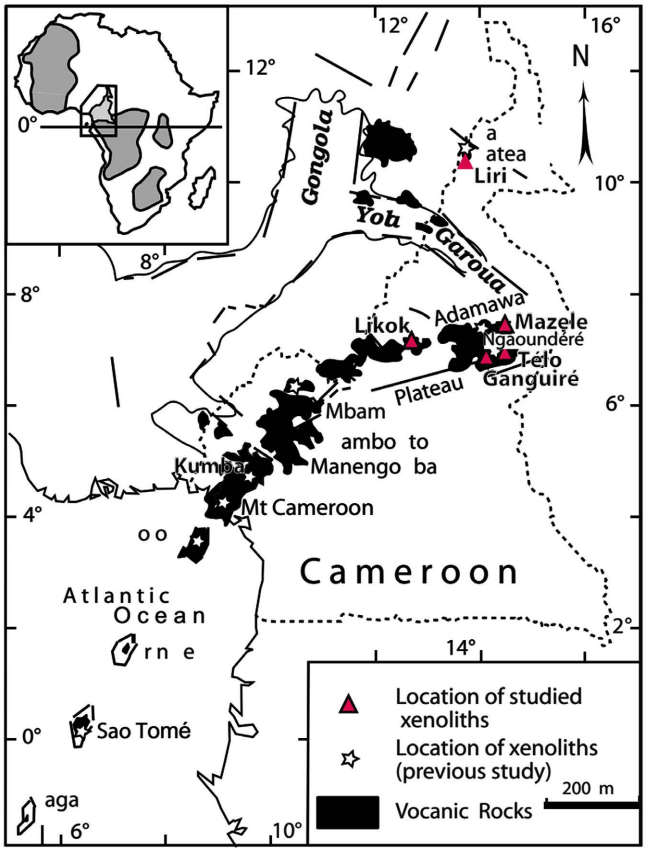

Figure 1. Location map of mantle xenoliths along the "Cameroon Volcanic Line" modified after [1].

with coeval and/or later magmatism and tectonic events such as plateau uplift and rifting [13]. New ultramafic deposits that are the subject of this study are harvested in the northern part of the LVC of Cameroon. Most are affected by cryptic metasomatism in which the chemical composition of the rock is changed by the addition or removal of elements. The theme discussed in this article concerns the mechanisms that are transmitted between the different mineral phases. More particularly, the study focuses on the comparison between the xenoliths of the mantle, mentioned in several places of the Cameroon volcanic line and on the Adamaoua plateau. These are precisely the locality of Liri (south of the Kapsiki plateau) and four localities of Adamaoua (Ganguiré, Mazele, Likok, Tello). The data relating to the sampling sites are reported in the following **Table 1**.

The example serving as support for this work is the continental domain of the Cameroon Volcanic Line, where certain volcanic edifices have emitted lava which contains peridotite xenoliths.

Xenoliths are fragments of mantle rock brought to the surface by magma during volcanic eruption. The upper mantle of the Earth is made up of peridotites at least in its superficial part. Peridotite xenoliths brought to the surface by alkaline basalts or kimberlites thus provide us with direct information on the processes and composition of the upper mantle.

Table 1. Sampling sites.

Localities	Mazele 1 (Maz 1)	Mazele 2 (Maz 2)	Ganguire (GA)	Liri	Tello 1 (TO1)	Likok (LO)	Tello 2 (TO2)
Geographic coordinates	N7˚33'55.84" E13˚48'24.44"	N7˚33'51.84" E13˚50'3.12"	N7˚05'25" E14˚02'35"	N10˚25'48" E13˚41'19"	N7˚13' E13˚40'	N7˚17'0.13" E13˚15'20.23	N7˚14' E13˚60'

These xenoliths constitute the major source of information concerning the state of stress, pressure and temperature prevailing in the deep mantle. They are thus a source of petrological and geochemical information which is not generally available on the Earth's surface

2. Geological Setting

2.1. Case of the Kapsiki Plateau

The Kapsiki Plateau (altitude ≈ 1000 m) is a volcanic area located at the far north of the "Cameroon Volcanic Line" [13]. The Precambrian basement of this zone is recovered by numerous trachyte needles and dykes, phonolite and rhyolite, and partially overlain by basalt flows. The age of the basalts is between 33.2 ± 1.3 Ma [14] and 27.0 ± 0.5 Ma [12]. Trachytes have been dated at 29.6 ± 0.6 Ma, [15] and 35.3 ± 2.4 Ma [15]. The age of the rhyolites is between 32 ± 0.5 Ma and 29.0 Ma [14]. The needles are more than fifty and rise above the Kapsiki plateau. Many of them are emplaced for the benefit of feeder dykes (Teki dyke). Needles from Roumsiki, Gouldé, Mogodé, Roumzu and Re Dilili, Omtémalé and Mchirgui are the most typical [16].

The presence of xenoliths in the Liri sector (south of the Kapsiki Plateau) was initially reported by [17]. According to the work of [16], it is proved that the structural and Geophysical (gravimetric and seismological) features of the granite-gneissic base complex are still poorly defined. The Liri sector is located along the Cameroon Line with a basement constituted of granite and gneiss. This basement is crossed by faults and locally covered by basaltic lava flows. The lava flows are broken up into the small centimetric blocks. The spinel-lherzolite xenoliths (size: 7 - 30 cm) with sub-rounded shapes were discovered in these dark basaltic lavas.

2.2. Case of the Adamaoua Plateau

Satellite documents [14] have made it possible to highlight alignments and lineamentary structures on the Adamaoua plateau. A main direction N70˚E emerges, called the "Adamaoua beam". This direction is a megaline several hundred kilometers long, which reflects the surface conditions and more or less materializes the deformations of the lithosphere under the influence of the stresses. It's formed during the Tertiary and then was uplifted up to 1 km relatively to the surrounding areas [18]. The plateau is limited by the N70˚E Adamaoua and Mbéré-Djerem faults [19]. The establishment of volcanism in this region is probably linked to these pan-African fractures [20]. Xenoliths crop out in basalt

flows in the shape of balls or metric-sized blocks. A few rare clinopyroxenite xenolites are encountered at the summits of the massifs. It is also necessary to note the presence of dolerites which form a planeze in certain sectors (case of Likok).

3. Results

3.1. Petrography

3.1.1. Petrography of Host Basanite

Host-lavas exhibit a massive structure. Phenocryst phases consist of euhedral to subhedral large olivine crystals (1.5 - 3 mm, 15 to 20 volume %), euhedral clinopyroxene (1 - 2 mm, 15%), Fe-Ti oxides (0.5 - 1 mm, 5%), set in a groundmass (60%) containing the same minerals and needle plagioclase microlites. The weathered surfaces are greenish gray in color, irregular with numerous multicentimeter to multimillimeter grains in relief giving the rock an irregular appearance due to meteoric alteration. The silicate minerals (olivine and pyroxene) remained in relief.

3.1.2. Petrography of Mantle Xenoliths

Basanitic lavas have entrained mantle peridotite xenoliths during their ascent to the Earth's surface. Ultramafic xenoliths sampled in these areas are spinel- and plagioclase-bearing [21] lherzolites. In our study only the following four minerals are observed.

Olivine

Olivine is the dominant mineral in these xenoliths. Some small crystals (≤0.5 mm or neoblasts) are sometimes nested between the orthopyroxene grains. They form by recrystallization at the periphery of granoclasts. Others of large size (>2 mm or porphyroclasts) contain small crystals of other minerals (cpx) (**Figure 2**) and having automorphic forms (curved limits). The olivine crystals present in places a fractured aspect along crack planes and locally show polygonal limits.

Orthopyroxene

Large orthopyroxene crystals are 3 to 6 mm in diameter and have curved outlines (**Figure 2**). Small polygonal crystals (0.5 - 1 mm) or undeformed neoblasts are present among the porphyroclasts of olivine crystals.

Clinopyroxene

Clinopyroxene crystals surround small olivine crystals with rounded edges. The clinopyroxene presents lamellae of exsolutions or inclusions of orthopyroxene. Two families are observed: one almost fibrous showing signs of fracturing and the other showing forms of annealing (**Figure 2**). Clinopyroxene (11-12) and orthopyroxene (15) crystals nest the olivine crystal (13). The large crystals of clinopyroxene present a distorted appearance and give the blade a destabilized structure. The mineralogical assemblage shows subautomorphic minerals. The clinopyroxene crystals appear here much more destabilized compared to the crystals of the other localities. Subautomorphic clinopyroxene and olivine crystals rarely form sharp joints.

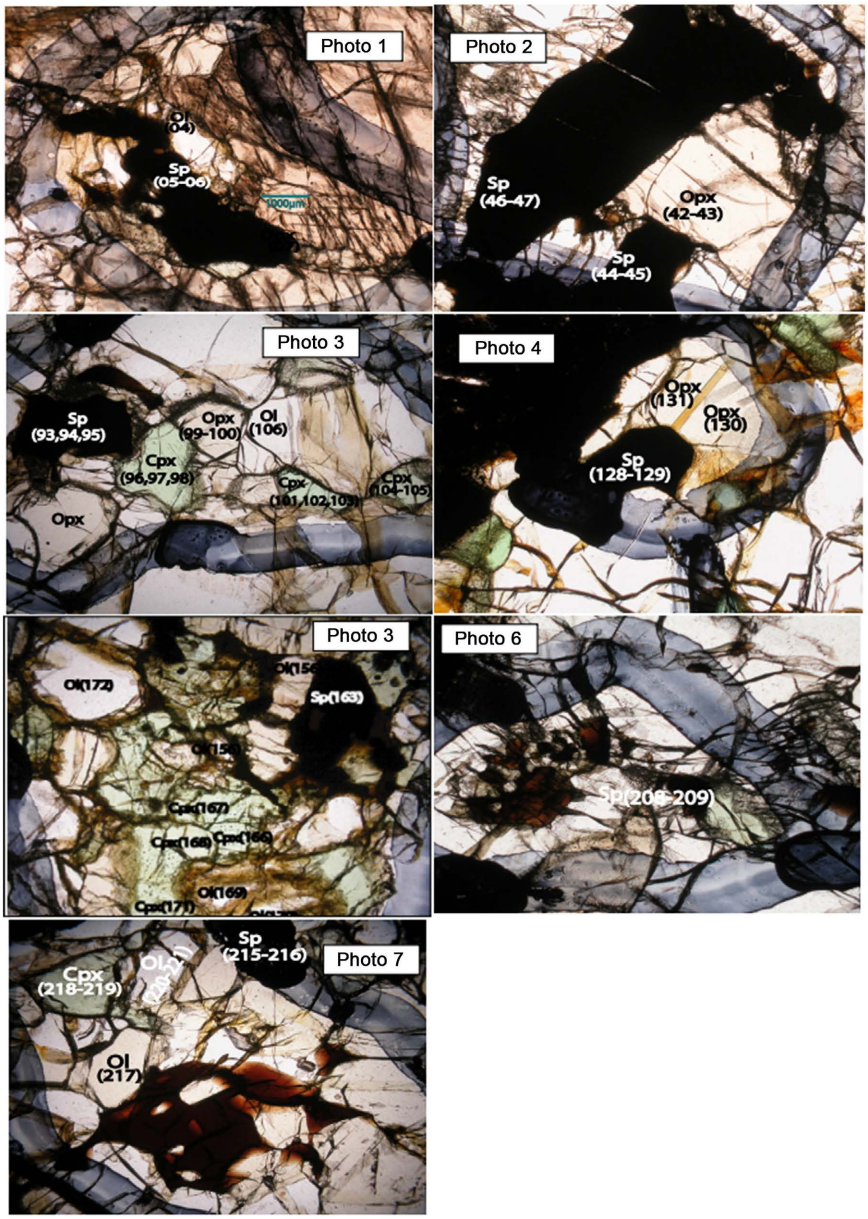

Figure 2. Microphotographs showing spongy clinopyroxenes and spinels scattered in the rocks and included in the silicate phases: the numbers for each mineral correspond to its analysis number (Photos 1 to 7 relate successively to the microphographies of Mazele1 (Maz1); Mazele 1 (Maz 2); Ganguire (GA); Liri, Tello 1 (TO1); Likok (LO) and Tello 2 (TO2)).

Spinel

Spinel grains arranged in a chain mold automorphic to subautomorphic orthopyroxene and clinopyroxene minerals. These grains are at times rounded or elongated (Figure 2) and give the blade a granoblastic texture. The contact between the spinel and the magmatic liquid leaves traces of oxidation, black spots. On the other hand, no sign of reaction between the different minerals in the xenoliths is observed. Overall, the bottom of the blade shows inclusions or infiltrations of the basaltic liquid. The automorphic spinels, arranged in clusters with

brown grain boundaries, have diameters that vary between 1 and 2 mm. They are arranged side by side with non-oriented olivine neoblasts with almost polygonal contours and half-millimeter dimensions.

3.2. Analytical Procedures

Mineral phases of the xenoliths and host basalt were analyzed using the CAMECA SX50 electronic microanalyzer at the Pierre and Marie Curie University in Paris (France) and in Canada. The samples analyzed are thin sections of rocks of different natures (basalts and xenoliths) and the analyzes are made on polished sections. Before each analysis, the samples are metallized with carbon. Radiation is then analyzed by spectrometers, each of which explores a specific range of wavelengths. Finally, the intensity of the radiation measured at the detector is compared with that produced under the same conditions by standards containing the desired elements at a known concentration. The final quantification of the elements (atoms, % by weight) is carried out by the PAP program of [22] which allows the correction of the analyses. The sensitivity threshold depends on the atomic number of the elements measured, the counting time (s), the voltage (Kv) and the current (nA) used. The analytical conditions are as follows: olivine: 15 kV, 40 nA, 20 s per element, except Si: 10 s; clinopyroxene: 15 kV, 40 nA, 20 s per element, except Ti: 30 s (Fe^{3+} recalculated according to [23]; orthopyroxene: 15 kV, 40 nA, 20 s per element, except Ti: 30 s (Fe^{3+} recalculated according to [23]; Fe-Ti oxides: 20 kV, 40 nA, 40 s per cell except Al and Cr: 30 s (Fe^{3+} recalculated from [24]; plagioclase: 15 kV, 10 nA, 10 sec; spinel: 10 kV, 80 nA, 40 s per element except Al and Cr: 30 s, and Zn and Ni: 15 s.

In the same way, the mineral phases of the xenoliths were also produced under the same conditions on the Cameca SX 100 microprobe of the Microsonde Ouest service in Brest (France).

3.3. Mineralogy

1) The mineralogy of the xenolites of the Cameroon Volcanic Line and the others localities based on the following four mineral phases.

Olivine

Olivine crystals from lherzolites (**Table 1**) are not zoned. Olivine crystals display a wide range of Fo (88.58 - 92.15). They are as rich in MgO (Fo~89.5) as that of the peridotite nodules of Sao Tomé ($Fo_{90\text{-}92}$) [25]; Bioko [26] and of the continental sector of "the Cameroon Ligne" [27] [28] [29]. The chemical compositions corroborate with recent data from Ngao Voglar in Adamaoua [30] which show that olivine crystals are relatively homogeneous and varies in composition from $Fo_{88.58}$to $Fo_{92.15}$ with Mg# of 89.1 - 89.8 [Mg# = 100 × Mg/(Mg + Fe^{2+})] and their NiO content varies from 0.03% - 0.5% and a low MnO value (0.11% - 0.2%). The CaO contents vary between 0.00% and 0.14%.

Clinopyroxene

The lherzolites containing chromium diopside (**Table 2**, **Figure 3**), nomen-

clature according to [31], low in TiO_2 (0.50% - 0.75%) with medium content in Cr_2O_3 (0.63% - 0.77%) and the content en MgO ~ 49%. Diopside compositions vary between ($Wo_{40.9\text{-}42.2}En_{50.4\text{-}51.6}Fs_{7.1\text{-}7.6}$).

Orthopyroxene

The lherzolites contain enstatite $Wo_{2.6}En_{86.2}Fs_{11.2}$ (**Table 3**, **Figure 3**), nomenclature according to [31] low in TiO_2 (<0.27%), Al_2O_3 (2.27% - 5.98%) and Cr_2O_3 (0.28% - 0.59%). Similarly, the chemical compositions of the orthopyroxenes from Mazélé are similar to the Ngao Voglar data with an enstatite rich in MgO (Mg# = 90.1; $En_{89\text{-}91}Wo_1Fs_{8\text{-}10}$), low in TiO_2 (0.02% - 0.12%) and Cr_2O_3 (0.28% - 0.43%), and a high content of Al_2O_3 (5.71% - 6.01%) and CaO (0.48% - 1.14%) (**Table 3**)

Spinel

The spinels (**Table 5**, **Figure 3**) of the different samples have contents which vary slightly in magnesium and chromium from one sample to another. The Cr_2O_3 contents vary between 9.0% and 9.6% and those of MgO are close to 20%. Their TiO_2 content is ~0.34%. The edges of the spinels in the sample show in places an enrichment in FeOT and a decrease in Cr_2O_3. The TiO_2 contents are low but these spinels are rich in Al_2O_3 (55.28 - 56.07).

Table 2. Chemical analyzes of olivines (% by weight and a.p.f.u. based on 4 oxygens).

Sample	MAZ1		MAZ2		TOb		GA		LIRI		TO1		LO		TO2	
Data Set	1/1.	4/1.	40/1.	41/1.	57/1.	58/1.	106/1.	118/1.	178/1.	179/1.	139/1.	143/1.	192/1.	197/1.	220/1.	221/1.
SiO_2	39.90	40.68	39.92	40.12	40.85	40.99	40.99	40.79	40.71	40.78	41.08	41.18	40.96	41.47	41.19	40.89
Al_2O_3	0.08	0.08	0.02	0.04	0.00	0.02	0.01	0.01	0.01	0.03	0.02	0.04	0.02	0.02	0.01	0.00
FeO	10.68	10.60	11.30	11.19	7.80	7.78	8.02	8.06	9.42	9.68	7.87	7.90	9.77	10.12	8.84	8.94
MnO	0.16	0.12	0.16	0.13	0.14	0.10	0.12	0.11	0.17	0.16	0.15	0.11	0.16	0.16	0.15	0.15
MgO	49.03	48.76	48.52	48.67	51.04	51.23	50.92	50.58	49.30	49.62	51.34	50.75	49.26	49.53	50.09	50.19
CaO	0.10	0.11	0.13	0.10	0.05	0.03	0.04	0.02	0.06	0.10	0.04	0.13	0.07	0.05	0.02	0.00
NiO	0.39	0.45	0.29	0.39	0.43	0.43	0.44	0.35	0.01	0.00	0.44	0.35	0.37	0.33	0.40	0.38
Sum	100.33	100.80	100.34	100.65	100.32	100.59	100.52	99.93	99.67	100.36	100.93	100.46	100.62	101.66	100.69	100.54
Si (a.p.f.u.)	0.982	0.994	1.329	1.336	0.991	0.992	0.993	0.994	0.999	0.995	0.991	0.997	0.998	1.001	0.999	0.994
Al	0.001	0.000	0.000	0.000	0.001	0.000	0.000	0.000	0.000	0.001		0.001	0.000		0.000	
Fe^{2+}	0.220	0.217	0.157	0.156	0.158	0.157	0.162	0.164	0.193	0.197	0.159	0.160	0.199	0.204	0.179	0.182
Mn	0.003	0.003	0.002	0.002	0.003	0.002	0.002	0.002	0.003	0.003	0.003	0.002	0.003	0.003	0.003	0.003
Mg	1.798	1.777	1.204	1.207	1.846	1.847	1.839	1.838	1.803	1.805	1.846	1.831	1.790	1.782	1.811	1.819
Ca	0.003	0.003	0.002	0.002	0.001	0.001	0.001	0.001	0.001	0.003	0.001	0.003	0.002	0.001	0.000	
Ni	0.008	0.009	0.004	0.005	0.008	0.008	0.008	0.007	0.000	0.000	0.009	0.007	0.007	0.006	0.008	0.007
Fa(%)	10.89	10.87	11.55	11.42	7.90	7.85	8.11	8.20	9.84	10.01	8.05	8.13	10.16	10.43	9.15	9.22
Fo	89.11	89.13	88.45	88.58	92.10	92.15	91.89	91.80	90.16	89.99	91.95	91.87	89.84	89.57	90.85	90.78

Table 3. Chemical analyzes of orthopyroxenes (% by weight and a.p.f.u. based on 6 oxygens).

Sample	MAZ1		MAZ2		Tob		GA		LIRI		TO1		LO		TO2	
Data Set	3/1.	7/1.	29/1.	30/1.	90/1.	60/1.	99/1.	100/1.	174/1.	165/1.	130/1.	131/1.	189/1.	190/1.	217/1.	226/1.
SiO_2	53.56	53.86	53.37	53.17	56.43	56.53	56.83	57.28	56.85	56.34	56.61	56.75	54.90	54.96	56.11	55.83
TiO_2	0.17	0.13	0.24	0.23	0.03	0.00	0.08	0.00	0.00	0.00	0.06	0.08	0.05	0.13	0.05	0.09
Al_2O_3	5.71	5.83	6.01	6.00	2.27	2.29	2.56	2.53	2.78	2.82	2.56	2.35	4.45	4.44	3.34	3.41
Cr_2O_3	0.39	0.40	0.43	0.41	0.37	0.39	0.43	0.43	0.31	0.28	0.50	0.40	0.28	0.31	0.29	0.29
FeO	6.67	6.98	6.90	7.08	4.92	5.07	5.18	5.15	6.16	6.25	5.03	4.89	6.04	6.40	5.60	5.83
MnO	0.19	0.16	0.14	0.13	0.11	0.14	0.15	0.13	0.19	0.17	0.10	0.14	0.13	0.13	0.13	0.09
MgO	31.96	31.54	31.52	31.13	35.21	35.10	35.03	34.88	34.38	33.76	34.56	34.99	33.15	32.99	34.30	34.36
CaO	1.14	1.19	1.29	1.24	0.49	0.49	0.55	0.51	0.47	0.83	0.60	0.59	0.79	0.74	0.40	0.45
Na_2O	0.19	0.18	0.19	0.17	0.00	0.00	0.07	0.04	0.07	0.10	0.09	0.09	0.08	0.08	0.06	0.08
K_2O	0.00	0.00	0.00	0.00			0.00	0.00	0.00	0.00					0.05	0.08
Sum	99.98	100.26	100.08	99.56	99.82	100.01	100.89	100.95	101.20	100.56	100.11	100.28	99.86	100.16	100.34	100.52
Fe_2O_3 (calc.)	2.21	1.35	1.92	1.42	1.33	1.12	0.88	0.00	0.64	0.88	0.20	0.74	1.09	0.93	0.61	1.40
FeO (calc.)	4.68	5.77	5.18	5.81	3.72	4.06	4.39	5.15	5.58	5.46	4.85	4.22	5.06	5.56	5.04	4.57
Sum (calc)	100.20	100.40	100.27	99.70	100.01	100.17	100.98	100.95	101.31	100.65	100.13	100.38	99.97	100.27	100.40	100.67
Si (a.p.f.u.)	1.852	1.861	1.847	1.852	1.933	1.935	1.932	1.947	1.934	1.931	1.936	1.935	1.893	1.893	1.921	1.908
Al^{iv}	0.148	0.139	0.153	0.148	0.067	0.065	0.068	0.053	0.066	0.069	0.064	0.065	0.107	0.107	0.079	0.092
Al^{vi}	0.084	0.099	0.092	0.099	0.025	0.028	0.034	0.048	0.046	0.045	0.040	0.029	0.074	0.073	0.055	0.045
Ti	0.005	0.003	0.006	0.006	0.001	0.000	0.002	0.000	0.000	0.000	0.001	0.002	0.001	0.003	0.001	0.002
Cr	0.011	0.011	0.012	0.011	0.010	0.011	0.012	0.012	0.008	0.008	0.014	0.011	0.008	0.008	0.008	0.008
Fe^{3+}	0.058	0.035	0.050	0.037	0.034	0.029	0.023	0.000	0.016	0.023	0.022	0.035	0.028	0.024	0.020	0.043
Fe^{2+}	0.135	0.167	0.150	0.169	0.107	0.116	0.125	0.146	0.159	0.157	0.122	0.105	0.146	0.160	0.140	0.124
Mn	0.006	0.005	0.004	0.004	0.003	0.004	0.004	0.004	0.005	0.005	0.003	0.004	0.004	0.004	0.004	0.003
Mg	1.647	1.625	1.626	1.617	1.798	1.792	1.775	1.767	1.744	1.725	1.762	1.779	1.704	1.694	1.750	1.750
Ca	0.042	0.044	0.048	0.046	0.018	0.018	0.020	0.019	0.017	0.031	0.022	0.022	0.029	0.027	0.015	0.017
Na	0.013	0.012	0.013	0.011	0.004	0.003	0.005	0.003	0.005	0.007	0.006	0.006	0.006	0.005	0.004	0.005
Mg#	0.924	0.907	0.916	0.905	0.944	0.939	0.934	0.924	0.917	0.917	0.935	0.944	0.921	0.914	0.926	0.934
Wo (mol.%)	2.23	2.35	2.54	2.46	0.92	0.92	1.04	0.96	0.88	1.58	1.14	1.11	1.53	1.43	0.76	0.86
En	87.27	86.64	86.60	86.32	91.73	91.47	91.18	91.29	89.83	88.93	91.26	91.51	89.16	88.72	90.74	90.39
Fs	10.50	11.01	10.86	11.22	7.35	7.61	7.79	7.75	9.30	9.49	7.60	7.38	9.30	9.85	8.50	8.75

2) Mineralogy of Mazele spinel lherzolites

The mineralogical analyzes are almost identical to those observed in other localities which constitute the north and the Cameroon Volcanic Line.

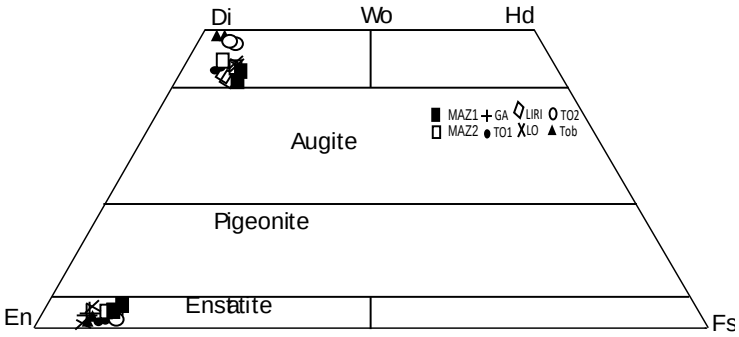

Figure 3. Composition of the pyroxenes of xenoliths according to [31].

Olivine

The Fo contents (91%) are relatively high, characteristic of mantle olivine (88 < Fo < 92) (**Table 2**). Nevertheless, their CaO contents are also high (0.0% and 0.13%) and are rather typical of phases having crystallized under low pressure and symptomatic of a volcanic origin [32]. The temperatures calculated using the thermometer of [33] are relatively high (1250˚C ± 50˚C) but consistent for the distribution of Mg, Fe and Mn.

Pyroxenes

The clinopyroxenes of xenoliths are diopsides ($Wo_{41.09\text{-}49.14}En_{47.25\text{-}51.82}Fs_{2.74.\text{-}7.82}$: [31] (**Table 3**), with Mg# ranging from 93.76 - 100. Their Cr_2O_3 contents (0.64% - 1.56%) qualify them as chromiferous diopsides (Cr a.f.u: >0.01: The fact that Mg#Cpx > Mg#Opx > FoOl, leaves to believe that these xenoliths are typical of residual peridotites [25] [26]). The TiO_2 and Al_2O_3 concentrations in the clinopyroxenes of these peridotites are high by 0.5 and, respectively with $Al^{VI} < 0.2$ and $Al^{IV} < 0.2$.

Orthopyroxenes (**Table 4**) are enstatites [31] with a composition varying from $_{Wo2.5\text{-}2.6}En_{86.3\text{-}86.5}Fs_{10.9\text{-}11.2}$. The Mg# of orthopyroxenes correlates with the Fo of olivines and indicates that Mg#Opx > Mg#ol [27] [34]. The orthopyroxenes of the peridotites have a high Al_2O_3 content (≥5%) compared to the contents obtained in the peridotites of TOb, GA and Liri.

Spinel

spinel (Mg, Fe^{2+}) $(Cr, Al, Fe^{3+})O_4$ (**Table 5**) is a mineral sensitive to chemical variations and plays, in particular, an important geochemical role in the partitioning of chromium. In the spinels analyzed, the Cr# content varies between 9.04% and 10.07%; the TiO_2 contents vary between 0.30% and 0.45%. Spinels occur in various habitus: in atoll, in automorphic grain, in complex association with other mineral phases.

3.4. Global Chemistry of Some Host Basalts

Note that the alkaline nature of these basalts has been confirmed by the study of certain trace elements and rare earths. The diagram in **Figure 3** shows the spectra of trace elements and rare earths normalized to chondrites from [35] of the host lavas of Ganguiré, [30], Mount Cameroon, [36] and the Kapsiki Plateau.

Table 4. Chemical analyzes of clinopyroxenes (% by weight and a.p.f.u. based on 6 oxygens).

Sample	MAZ1		MZ2		Tob		GA		LIRI		TO1		LO		TO2	
Data Set	2/1.	8/1.	31/1.	32/1.	62./1.	66/1.	96/1.	97/1.	166/1.	167/1.	132/1.	133/1.	194/1.	195/1.	218/1.	219/1.
SiO_2	50.36	50.82	50.55	50.49	53.12	53.44	53.55	53.49	52.28	51.59	53.20	53.15	51.88	51.99	51.90	52.08
TiO_2	0.76	0.74	0.62	0.50	0.08	0.03	0.08	0.15	0.26	0.32	0.28	0.28	0.51	0.46	0.49	0.52
Al_2O_3	7.74	7.64	7.53	7.55	3.04	2.91	3.51	3.59	5.14	5.87	4.48	4.37	6.70	6.53	5.91	5.90
Cr_2O_3	0.67	0.77	0.71	0.68	1.08	0.93	1.04	1.13	0.93	1.01	1.56	1.56	0.78	0.73	0.95	0.96
FeO	3.93	4.03	4.20	4.28	1.61	1.63	2.01	1.79	2.64	2.76	2.03	1.94	2.65	2.73	2.00	1.92
MnO	0.09	0.12	0.10	0.12	0.06	0.10	0.12	0.04	0.10	0.10	0.10	0.06	0.10	0.10	0.04	0.11
MgO	15.82	16.06	16.26	16.11	16.76	16.97	16.66	16.56	15.84	15.66	15.88	15.79	15.21	15.50	14.99	15.24
CaO	18.49	18.45	18.12	18.03	22.77	22.84	22.49	22.50	21.50	21.42	21.20	21.12	20.76	20.26	21.69	21.72
Na_2O	1.56	1.58	1.59	1.52	0.96	0.88	1.15	1.21	1.37	1.36	1.71	1.80	1.64	1.61	1.58	1.53
Sum	99.42	100.20	99.67	99.28	99.49	99.72	100.60	100.47	100.08	100.15	100.49	100.13	100.31	99.94	99.54	100.00
Fe_2O_3 (calc.)	2.51	2.53	3.20	2.68	1.75	1.53	2.07	1.89	2.37	2.81	1.83	1.94	1.74	1.43	1.51	1.54
FeO (calc.)	1.68	1.75	1.31	1.86	0.03	0.25	0.15	0.09	0.51	0.24	0.38	0.19	1.08	1.44	0.64	0.54
Sum(calc)	99.72	100.53	100.02	99.58	99.66	99.87	100.81	100.66	100.30	100.40	100.67	100.32	100.39	100.06	99.69	100.18
T-Site																
Si (a.p.f.u.)	1.825	1.828	1.825	1.832	1.927	1.934	1.921	1.921	1.886	1.861	1.924	1.929	1.867	1.875	1.882	1.879
Al^{iv}	0.175	0.172	0.175	0.168	0.073	0.066	0.079	0.079	0.114	0.139	0.076	0.071	0.133	0.125	0.118	0.121
Sum	2.000	2.000	2.000	2.000	2.000	2.000	2.000	2.000	2.000	2.000	2.000	2.000	2.000	2.000	2.000	2.000
M1-Site																
Mg	0.695	0.696	0.699	0.694	0.871	0.861	0.839	0.838	0.783	0.769	0.777	0.778	0.737	0.737	0.766	0.772
Fe	0.046	0.047	0.035	0.051	0.001	0.007	0.004	0.002	0.014	0.006	0.055	0.053	0.029	0.039	0.017	0.012
Al^{vi}	0.156	0.151	0.145	0.155	0.057	0.058	0.069	0.073	0.105	0.111	0.115	0.116	0.151	0.153	0.134	0.130
Fe^{3+}	0.068	0.069	0.088	0.073	0.048	0.042	0.056	0.051	0.064	0.076	0.011	0.006	0.047	0.039	0.041	0.044
Ti	0.021	0.020	0.017	0.014	0.002	0.001	0.002	0.004	0.007	0.009	0.008	0.008	0.014	0.012	0.013	0.014
Cr	0.019	0.022	0.020	0.020	0.031	0.027	0.030	0.032	0.027	0.029	0.045	0.045	0.022	0.021	0.027	0.027
Sum	1.004	1.005	1.004	1.006	1.010	0.995	1.000	1.000	1.000	1.000	1.011	1.005	1.000	1.001	0.999	0.999
M2-Site																
Ca	0.718	0.711	0.701	0.701	0.885	0.886	0.864	0.865	0.831	0.828	0.821	0.821	0.800	0.783	0.842	0.840
Na	0.110	0.110	0.112	0.107	0.068	0.061	0.080	0.084	0.096	0.095	0.119	0.126	0.115	0.112	0.111	0.107
Mg	0.160	0.166	0.176	0.178	0.035	0.054	0.052	0.049	0.069	0.074	0.079	0.076	0.079	0.097	0.044	0.048
Fe	0.010	0.010	0.008	0.012	0.000	0.000	0.000	0.000	0.001	0.001	0.006	0.005	0.003	0.005	0.001	0.001
Mn	0.003	0.004	0.003	0.004	0.002	0.003	0.004	0.001	0.003	0.003	0.003	0.002	0.003	0.003	0.001	0.003
Sum	1.000	1.000	0.999	1.000	0.990	1.005	1.000	1.000	1.000	1.000	1.028	1.030	1.000	1.000	1.000	0.999
V(cell)	434.10	434.07	433.72	433.87	433.13	439.62	437.03	436.93	436.10	436.03	435.66	435.57	434.89	434.68	435.51	435.09
V(M1)	11.43	11.44	11.43	11.44	11.59	11.77	11.67	11.66	11.58	11.55	11.52	11.51	11.48	11.49	11.53	11.52
Alvi/Aliv	0.89	0.88	0.83	0.92	0.79	0.87	0.88	0.91	0.92	0.80	1.51	1.62	1.13	1.22	1.13	1.07
Mg#	0.94	0.94	0.96	0.94	1.00	0.99	1.00	1.00	0.98	0.99	0.93	0.94	0.96	0.95	0.98	0.98
Cr#	0.05	0.06	0.06	0.06	0.19	0.18	0.17	0.17	0.11	0.10	0.19	0.19	0.07	0.07	0.10	0.10
Wo(Ca)	42.36	41.90	41.09	41.09	48.05	47.78	47.51	47.89	43.55	43.05	47.16	47.30	47.11	46.00	49.14	48.80
En (Mg)	50.45	50.76	51.30	51.10	49.20	49.40	48.97	49.06	51.63	51.82	49.16	49.21	48.02	48.99	47.25	47.64
Fs (Fe^{2+Fe3+}Mn)	7.19	7.34	7.61	7.82	2.74	2.82	3.52	3.05	4.83	5.12	3.68	3.49	4.87	5.01	3.61	3.57

Table 5. Chemical analyzes of spinels (% by weight and a.p.f.u. based on 32 oxygens).

Samples	MAZ1		MAZ2		GA		Liri		TO1		LO		TO2	
Data Set	5/1.	6/1.	44/1	45/1	93/1	94/1	163/1	164/1	128/1	129/1	208/1	209/1	215/1	216/1
SiO_2	0.11	0.08	0.12	0.13	0.02	0.06	0.06	0.07	0.02	0.36	0.05	0.07	0.04	0.07
TiO_2	0.31	0.38	0.30	0.34	0.12	0.08	0.15	0.16	0.18	0.21	0.12	0.13	0.10	0.11
Al_2O_3	56.06	56.07	55.76	55.80	40.88	40.82	46.60	46.35	34.64	34.91	57.82	57.84	55.52	55.54
Cr_2O_3	9.39	9.41	9.28	9.23	29.28	29.28	18.93	19.40	32.81	32.67	10.39	10.26	13.03	12.93
FeO	12.66	12.86	13.22	13.50	10.51	11.01	13.96	14.05	13.04	13.21	10.25	10.17	9.77	9.75
MnO	0.11	0.11	0.10	0.02	0.14	0.07	0.14	0.14	0.12	0.15	0.13	0.08	0.06	0.08
MgO	20.24	20.57	20.10	19.89	18.42	18.36	19.73	19.35	17.55	17.34	21.20	21.40	20.45	20.85
CaO	0.00	0.00	0.02	0.02	0.00	0.00	0.00	0.00	0.00	0.00	0.00	0.00	0.03	0.00
Na_2O	0.02	0.03	0.02	0.02	0.01	0.00	0.00	0.00	0.00	0.00			0.00	0.00
NiO	0.39	0.42	0.43	0.37	0.25	0.20	0.33	0.29	0.20	0.24	0.36	0.35	0.35	0.30
P_2O_5	0.00	0.00	0.02	0.00	0.01	0.04	0.00	0.00	0.00	0.00	0.00	0.05	0.00	0.00
Sum	99.29	99.94	99.36	99.32	99.64	99.92	99.90	99.82	98.57	99.10	100.31	100.35	99.34	99.64
Fe_2O_3 (calc)	3.42	3.98	3.78	3.59	0.64	0.84	5.48	4.95	3.23	2.38	1.88	1.91	9.02	8.64
FeO (calc)	9.58	9.28	9.82	10.27	9.94	10.26	9.03	9.60	10.14	11.06	8.55	8.45	0.82	1.23
CALC. TOTAL	99.63	100.34	99.74	99.68	99.69	99.96	100.45	100.32	98.90	99.34	100.50	100.54	99.34	99.64
Si	0.022	0.018	0.026	0.028	0.005	0.012	0.013	0.015	0.005	0.083	0.010	0.014	0.009	0.015
Ti	0.049	0.059	0.047	0.053	0.020	0.013	0.024	0.027	0.032	0.036	0.018	0.021	0.016	0.018
Al	13.782	13.695	13.725	13.755	10.703	10.671	11.817	11.799	9.398	9.430	13.971	13.954	13.671	13.615
Cr	1.549	1.542	1.533	1.526	5.142	5.135	3.220	3.313	5.970	5.920	1.684	1.661	2.152	2.127
Fe^{3+}	0.537	0.621	0.595	0.565	0.102	0.126	0.887	0.805	0.559	0.411	0.290	0.295	0.130	0.192
Fe^{2+}	1.672	1.608	1.715	1.797	1.850	1.917	1.624	1.733	1.951	2.120	1.466	1.447	1.577	1.503
Mn	0.019	0.019	0.017	0.004	0.027	0.014	0.026	0.026	0.024	0.030	0.022	0.014	0.011	0.014
Mg	6.295	6.356	6.258	6.201	6.100	6.070	6.330	6.231	6.024	5.924	6.479	6.530	6.371	6.465
Ca	0.000	0.000	0.004	0.003	0.000	0.000	0.000	0.000	0.000	0.000	0.001	0.000	0.007	0.000
Na	0.010	0.012	0.007	0.006	0.004	0.000	0.000	0.000	0.000	0.000	0.000	0.000	0.001	0.000
Ni	0.066	0.070	0.072	0.063	0.044	0.037	0.057	0.051	0.038	0.045	0.059	0.058	0.058	0.050
Mg#	0.79	0.80	0.78	0.78	0.77	0.76	0.80	0.78	0.76	0.74	0.82	0.82	0.80	0.81
Cr#	0.10	0.10	0.10	0.10	0.32	0.32	0.21	0.22	0.39	0.39	0.11	0.11	0.14	0.14

It is observed that the trace element and rare earth spectra of these different lava units show similar trends. But we note the presence of a negative anomaly in Th and positive anomalies in U and Sr in the host lavas of Ganguiré. They all show a slight anomaly positive in Eu and negative in Dy. The spectra of these lavas are more enriched in light rare earths (La, Ce, Pr and Nd) compared to heavy rare earths (Dy, Yb and Lu) which is a characteristic of alkaline lava (**Figure 4**).

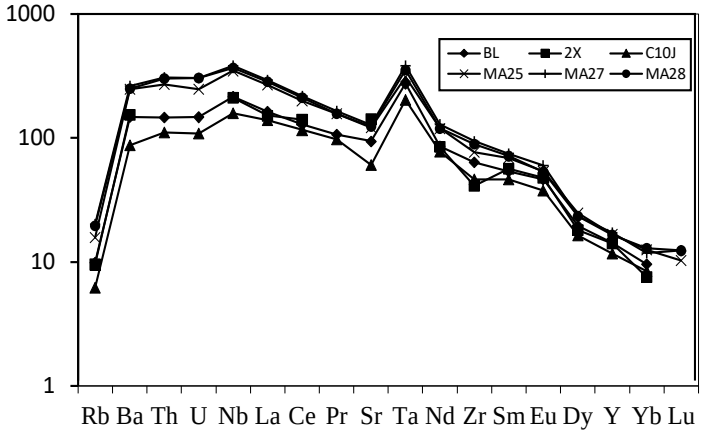

Figure 4. Incompatible element patterns for the host basalts of Liri (BL), Ganguiré (Mazélé; MA), Mount Cameroon (C10J), Kapsiki plateau (2X), normalized to the mean of the chondrites of [35].

4. Discussion

Exchange reactions and equilibrium state

Mineralogically, xenoliths contain four mineral phases: olivine (ol), orthopyroxene (opx), clinopyroxene (cpx) and an aluminous phase, spinel (sp). The elements are not randomly distributed among the various mineral phases. Indeed, they are governed by a set of exchange and transfer reactions governed by strict thermodynamic laws. Here, we will review a number of these reactions, which should later make it possible to characterize the chemical composition of the upper mantle of each region and test the state of equilibrium of the phases between them.

4.1. Exchange Reactions

Fe-Mg exchange between olivine and orthopyroxene

In the case of these peridotites, visual observation under a microscope reveals that olivine and orthopyroxene constitute more than 70% - 90% of the modal composition, and are chemically very close to the FeO-MgO-SiO_2 (FMS) system. We can therefore characterize the chemical variation of the Fe and Mg systems with the olivine/orthopyroxene couple.

According to the work of [37], the Fe-Mg exchange between olivine and orthopyroxene can be described by assuming a monosite ideal solution behavior for these two phases at high temperatures (>1000˚C), but such a model also remains valid for lower temperatures (800˚C - 900˚C) especially when studying the field of interest around Fo = 90, except for a few cases of the values of TOb and TO1 which slightly exceed (Fo = 92) and that of MAZ whose values are lower (Fo = 88). We can therefore use the following reaction to express this exchange

$$Mg_2SiO_4 + Fe_2Si_2O_6 <==> Mg_2Si_2O_6 + Fe_2SiO_4$$

Fo(ol) Fs(opx) En(opx) Fa(ol)

The partition coefficient is expressed as follows for the exchange of one atom

for another:

$$K_D = ((X_{Fe})_{ol} * (X_{Mg})_{opx})/((X_{Mg})_{ol} * (X_{Fe})_{opx}$$

For application to the natural system, considering that the exchange between Mg and Fe is limited to the octahedral sites not occupied by Ca, Na, Cr, Al (the other elements can be neglected), the concentrations corresponding to the FMS system can be estimated as being equal to:

$$(X_{Mg})_{ol} = (Mg/Mg + Fe^{2+})_{ol} \qquad (X_{Fe})_{ol} = 1 - (X_{Mg})_{ol}$$

$$(X_{Mg})_{opx} = (Mg/Mg + Fe^{2+})_{opx} \qquad (X_{Fe})_{opx} = 1 - (X_{Mg})_{opx}$$

Knowing the ratios (Mg/Mg + Fe) of olivine and orthopyroxene of peridotites we can construct the Roozeboom diagram (Mg/Mg + Fe) olversus (Mg/Mg + Fe) opx and determine the partition coefficient at compare with the theoretical model. Figure 5 shows a correlation between olivine and orthopyroxene, indicating partition coefficients greater than 1 with the exception of peridotites from Ganguirét having a mean value ≤0.94). The forsterite content of olivine ranges from 88 - 92. This range of values is typical of mantle rocks.

Al-Cr exchange between pyroxene and spinel

Since Al Indeed, [38] experimentally found by measuring the interatomic distance that, in pyroxene, Al occupies both tetrahedral and octahedral sites, while Cr only occupies octahedral sites. The presence of Na in pyroxene also requires an equivalent quantity of trivalent ions (Al, Cr and Fe^{3+}) to maintain the electroneutrality of the phase. The proportion of these three species is relatively constant in the presence of a given aluminous phase for the peridotites of the mantle [39]. In our case, for the spinel facies, the concentration of trivalent Fe in the pyroxenes is very low and no significant value can be calculated from the results of the microprobe analyses.

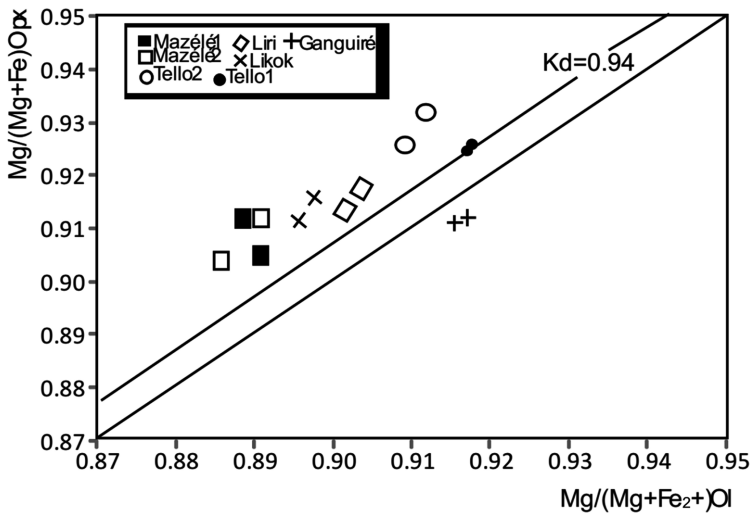

Figure 5. Roozeboom type diagram for the exchange of Fe—Mg between olivine and orthopyroxene which are two phases of the reaction, the value 0.94 corresponds to the constant kd [35].

Reaction in order of importance is:

$$(Mg, Fe)_3Al(AlSi_3O_{12}) + 1/2(Mg, Fe)Cr_2O_4 <==> (Mg, Fe)_3Cr(AlSi_3O_{12}) + 1/2(Mg, Fe)Al_2O_4$$
$$\text{(opx)} \qquad \text{(sp)} \qquad \text{(opx)} \qquad \text{(sp)}$$

The experiment shows that by measuring the interatomic distance in pyroxene, Al occupies both tetrahedral and octahedral sites, while Cr only occupies octahedral sites. The presence of Na in pyroxene also requires an equivalent quantity of trivalent ions (Al, Cr and Fe^{3+}) to maintain the electroneutrality of the phase. The proportion of these three species is relatively constant in the presence of a aluminous phase for the peridotites of [40]. In our case, for the spinel facies, the concentration of trivalent Fe in the pyroxenes is very low and no significant value can be calculated from the results of the microprobe analyses.

In summary, to express the Al-Cr exchange between orthopyroxene and spinel, we should calculate the amount of Al in the octahedral site not associated with Na, *i.e.* $VI^{Al*} = (Al - Cr - Na)/2$. Tetrahedral aluminum is equal to $IV^{Al} = (Al + Cr - Na)/2$. A Roozeboom diagram $(Cr/Cr + Al)Sp - (Cr/Al^{IV})$ Opx is used to describe this exchange appropriately. The trend in **Figure 4** implies spinel non-ideality at the Y site for a Cr-Al substitution. This observation is in agreement with the experimental and theoretical data which show that the simple model of regular solution is well suited to describe this Al-Cr partition between spinel and orthopyroxene.

X2 = X1/(X1 + K(1 − X1) exp(WG(2X1 − 1)/RT for fixed T with X1 = (Cr/Cr + Al)spX2 = (2Cr/Al + Cr − Na)opx; X1 and X2 being respective concentrations of Cr in spinel and orthopyroxene. WG(2X1 − 1)RT being the excess energy with a value of 11.3 kJ for the Margules parameter WG, from [41]. This expression allows us to calculate the theoretical Al-Cr partition between spinel and orthopyroxene which is represented in the inset in **Figure 6** by asymmetrical curves contrasting with those of **Figure 6**. The majority of the points lie on a curve corresponding to an equilibrium constant practically equal to 2.5.

Al-Cr exchange between the two pyroxenes

The Al-Cr exchange between the two pyroxenes is well described by an ideal solution model [42], using the couple (Cr/Al^{IV})cpx and (Cr/Al^{IV})opx, and an equilibrium constant written as follows:

$$K_D = (X_{Al})_{opx}(X_{Cr})_{cpx}/(X_{Cr})_{opx}(X_{Al})_{cpx}$$
$$\text{avec } (X_{Cr})_{opx} = 2Cr/Al + Cr - Na$$
$$(X_{Al})_{opx} = 1 - (2Cr/Cr + Al - Na)$$

Figure 7 indicates that the equilibrium constant is significantly different from unity and varies from 1.5 to 3.5 except for the samples from Ganguiré and Tello 2 whose distribution coefficients Kd are greater than 3.5. The Cr and Al contents of clinopyroxene are about twice as high as those of orthopyroxene. The correlation observed here confirms what we have seen in the previous diagrams: all the samples of peridotite show a good state of equilibrium, and are therefore completely characteristic of the normal mantle.

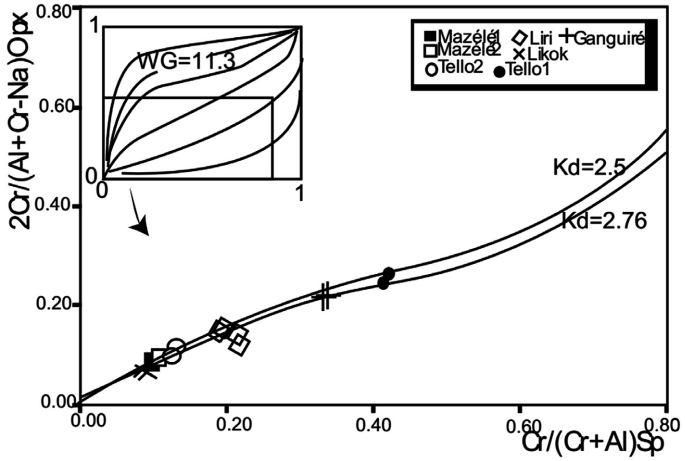

Figure 6. Roozeboom diagram for Cr—Al exchange between spinel and orthopyroxene. The regular solution model was calculated at 900˚C (inset) with an excess energy of 11.3 KJ [40]) for the Cr—Al interaction at Y sites of spinel.

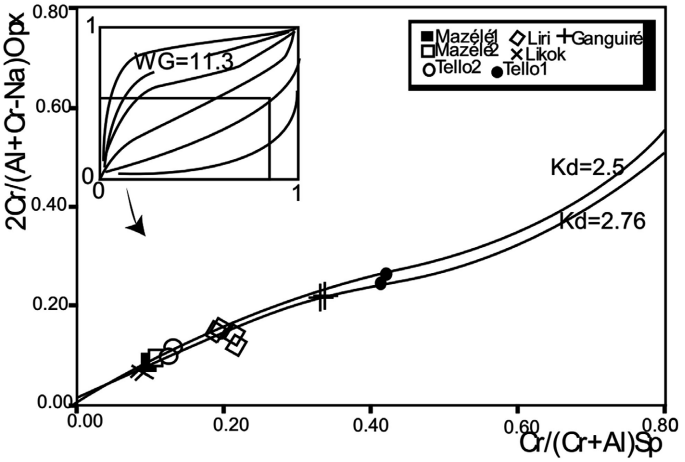

Figure 7. Roozeboom diagram for the exchange of Cr—Al between the two pyroxenes. Only Cr and Al in non-bonded octahedral site are taken into account in the exchange.

Diagram (Mg/Mg + Fe^{2+})sp versus (Cr/Cr+Al)sp

It is well known that spinel cannot be considered as a single-site ideal solution with respect to Fe—Mg substitution due to interactions between X and Y sites, called reciprocal effects. The interactions of the cations (Al, Cr) in the Y sites of spinel with the cations (Fe, Mg) in the X sites can be described by the following reaction:

$$FeAl_2O_4 + MgCr_2O_4 == FeCr_2O_4 + MgAl_2O_4$$

Since spinel is a Cr-rich mineral compared to other phases in which Cr is almost trace, the ratio (Cr/Cr + Al)sp reflects that of the system and controls (Mg/Mg + Fe^{2+})sp. An autocorrelation is observed in **Figure 8**. This figure which shows the reciprocal nature of the spinel solution, also illustrates a significant variation in (Cr/Cr + Al) of the system.

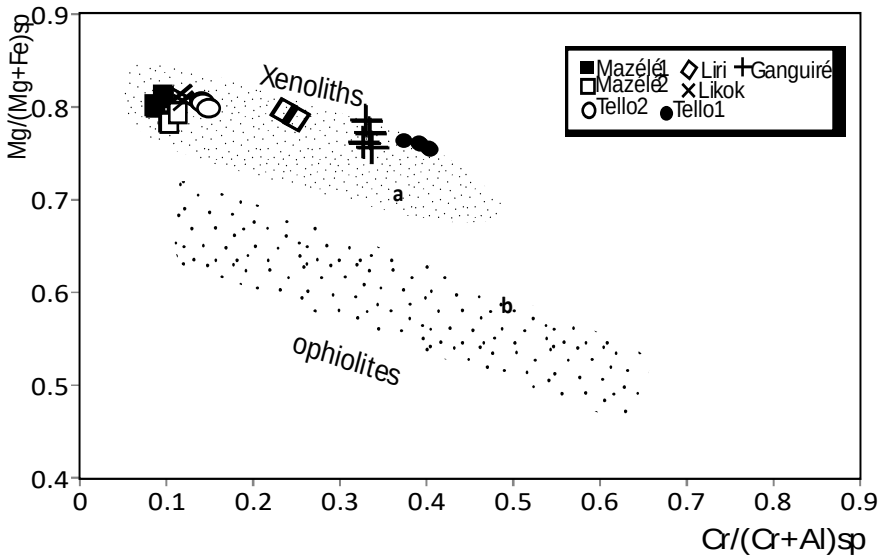

Figure 8. Mg#-Cr# autocorrelation diagram for the spinel phase. The ophiolite reference is reported from [34]. (a) Domain of ultrabasic enclaves (Lherzolites and Harburgites) in basic lavas [42]; (b) Domain of ultrabasic rocks in ophiolites [41].

We can clearly see a well-defined domain for the xenoliths studied which is placed above that corresponding to the ophiolitic massifs (field of ophiolites according to [41]. This is the normal position of spinel peridotites typical of a lithospheric mantle sampled by alkaline magma quenched within hours. This characteristic leads us to believe that these peridotites are not fragments of an ultrabasic body (tectonic scale) in the continental crust, but that they have a deep origin in the mantle. This observation is completely analogous with that of other xenoliths in the alkaline basalts of Cameroon [27]. The difference between the position of xenoliths and ophiolites was explained by the kinetics of this exchange reaction [43].

4.2. Transfer Reactions

Balance state

Exchange reactions are well suited for verifying the global equilibrium state of paragenesis, whereas transfer reactions are more suitable for estimating equilibrium conditions. There are two types of transfer reactions classically applied to pyroxenes for spinel facies peridotites: one concerns the mutual solubility of orthopyroxene and clinopyroxene, and the other concerns the solubility of aluminum in buffered orthopyroxene by the spinel:

$$\text{En(opx)} <=> \text{En(cpx)} \text{ et } \text{Di(opx)} <=> \text{Di(cpx)}$$

$$\text{and } \text{Py(opx)} + \text{Fo(ol)} <==> \text{En(opx)} + \text{Sp(sp)}$$

The theoretical equilibrium curves were calculated under different pressures according to the different thermometers (Bertrand *et al.*, 1987; Bertrand and Mercier, 1985; Benoît, 1987).

The combination of these reactions is also a particularly suitable tool for test-

ing the state of equilibrium of the pyroxenes of ultrabasic parageneses [44].

Equilibrium conditions

Previous studies have shown us that the xenoliths studied are completely in equilibrium. This therefore allows us to estimate the physical conditions to which they were subjected just before the eruptions, using the transfer reactions described by the thermodynamic laws.

Temperature

Several geothermometers have been calibrated from experimental data and/or data from the natural system [40], but the choice among these thermometers is not particularly easy. The fundamental problem for thermometry is the extrapolation of P-T from the experimental region when determining the pressures and temperatures of fairly simple synthetic systems to the complex natural compositions of xenoliths. Here we will arbitrarily consider three thermometers (one of which is for an exchange reaction) to determine the equilibrium conditions and check the consistency of the results.

4.3. Fe—Mg Exchange between Olivine and Spinel

[45] [46] calibrated a thermometer for the Fe—Mg exchange reaction between olivine and spinel:

$$T\ (^{\circ}K) = (4250(Y_{Cr})_{sp} + 1343)/(\mathrm{Ln}K_D + 1.825(Y_{Cr})_{sp} + 0.571)$$

où $(Y_{Cr})_{sp}$= (Cr/Cr + Al)sp; K_D is an equilibrium constant

$$K_D = (X_{Mg})_{ol} * (X_{Fe})_{sp}/(X_{Mg})_{sp} * (X_{Fe})_{ol}$$

Given that the forsterite content of the olivine of the peridotites in the samples is between 88% and 92% and that the Fe^{3+} concentration of the spinel is on the whole very low, it seems reasonable to use this thermometer. The calculation gives a temperature of 845˚C - 1050˚C.

It is well known that as with all thermometers based on exchange reactions, this thermometer is easily disturbed. The temperatures calculated from this thermometer therefore reflect the equilibrium conditions of the last thermal state, that is to say when the peridotites were sampled by the magma which brought them up.

Pression

Pressure estimation remains problematic. Although some calibrations using the solubility of aluminum in orthopyroxene [39] or of calcium in orthopyroxene [40] have been proposed, there is no reliable and precise geobarometer for spinel facies mantle rocks.

As we did not observe garnet in the samples, it is plausible to consider a maximum pressure of 2.5 GPa and a minimum pressure of 0.9 GPa can also be estimated [46] due to the absence of plagioclase.

Other parameters are also sensitive to pressure, in particular the constant Na (Opx)/Na(Cpx) for the sodium exchange reaction between pyroxenes, and Ca in olivine buffered by the couple of reactions between the two pyroxenes. No calibration exists for Na but the Ca (Ol) geothermobarometer has been studied ex-

perimentally for CMS and CFMS systems for Fe = 0.16. The problem is the quality of analyzes of this trace element. As the silicon of spinel is a good thermometer, it is practical to study these two traces simultaneously with spinel, despite its empiricism. Calculation indicates that pressures from diopside are outside the allowable range (0.9 - 2.5 GPa) we mentioned, while pressures from enstatite are more reasonable (1.4 - 2 GPa). To calculate the pressure, we used the following [47] formula:

$P(kbar) = 771.48 + 4.956.AlT - 28.756.Fe^{2+}M1 - 5.345.Fe^{3+} + 56.904.AlM1 + 1.848.Ti + 14.825.Cr - 773.74.Ca - 736.57.Na - 754.81.MgM2 - 763.20.Fe^{2+}M2 + - 759.66Mn - 1.185\ (MgM2)2 - 1.876.(FeM2)2.$

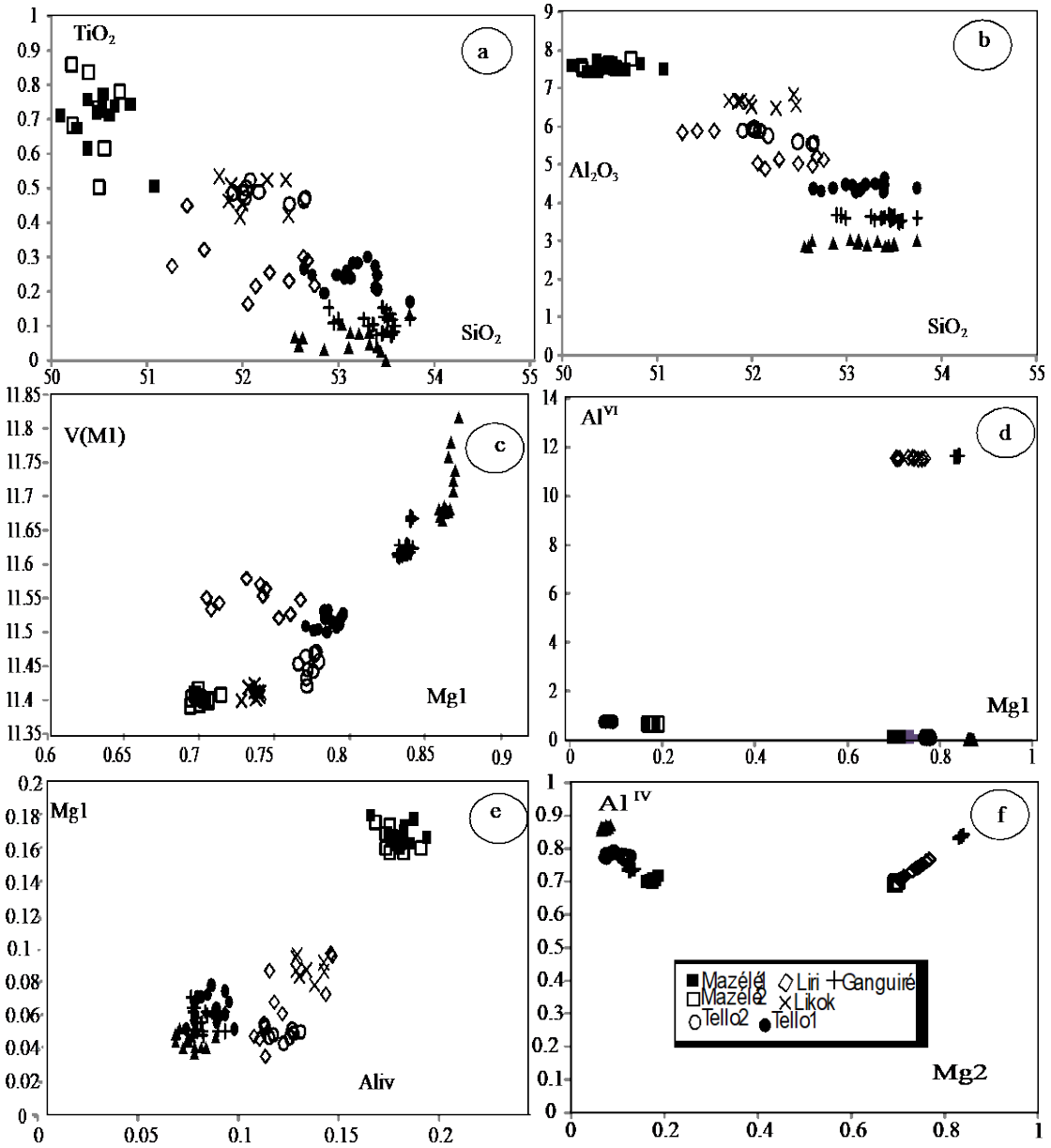

Figure 9. Diagram of variation of SiO_2 vs TiO_2, SiO_2 vs Al_2O_3, V(M1) vs Mg1, Al^{IV} vs Mg1, Al^{IV} vs Mg1 and Mg2 vs Al^{IV} in the cpx of the different localities.

4.4. Behavior of Some Major and Trace Elements in Clinopyroxens

Here we observe a characteristic negative correlation of melt residue between the TiO_2 and SiO_2 content for the clinopyroxenes (**Figure 8**). All samples follow the evolution of the trend. The TiO_2 contents decrease from the high cpx values of MAZ2 and MAZ1 ≥ 0.7, to the average values of LO, TO_2 and Liri varying between 0.2 and 0.5. The lowest TiO_2 values occupying the bottom of the slope are those of TiO_2 present in the Cpx of Tob and To1 whose values are almost zero < 0.1. The same trend is observed with the evolution of the Al_2O_3 content as a function of SiO_2 which shows a negative correlation leaving higher values (7 - 8) of MAZ1 and MAZ2. On the other hand, the TiO_2 and Al_2O_3 contents are roughly anti-correlated with SiO_2 (behavior of a fusion residue). Their anticorrelations reflect their low levels. The proportion of Cpx can vary significantly within the same series or between the xenoliths chosen. The M1 and M2 octahedral sites of the Cpx have a very marked difference in terms of morphology. The variation of V(M1) as a function of Mg1 makes a positive correlation (**Figure 9c**). This testifies to a state of equilibrium between the minerals and their appropriate sites [47] [48]. Similarly for the other chemical elements Mg1, Al^{iv} which fill the same sites, we observe tendencies of a positive correlation contrary to the elements which do not share the same site (Al^{iv}, Mg2). A high Mg1 content in the M1 site automatically leads to an increase in the Al^{iv} content (**Figure 9**).

5. Conclusions

The study of the mineral phases of spinel lherzolites from Mazélé in particular and the Adamaou plateau in general present results which corroborate with other spinel lherzolites from the continental sector of the Cameroon Volcanic Line. Of the above, the homogeneous character of the texture, mineralogy and chemistry is manifested in the mantle xenoliths of lherzolite of the volcanic massif of Mazélé and others northen xenoliths, reflecting the stability of the lithospheric mantle in the northern continental domain of the Cameroon volcanic line. The mineralogical assembly of the four phases (olivine, clinopyrones, orthopyroxe and spinel) reflects the balance [49] [50]. The homogeneity of the physical conditions (P, T) as well as the homogeneity of the texture suggest that the peridotites in enclaves in the alkaline basalts of the regions located on the Adamaoua and Kapsiki plateau undoubtedly prove to be from an upper mantle level mostly located between 0.6 and 1.4 GPa (22 - 45 km) for a temperature of 1000˚C at the time of the eruption.

Such mechanisms in mantle rocks can be related to low degrees of partial melting of liquids from a fertile lherzolite to a melt residue [51] [52]. In some spinel-rich porphyroclastic lherzolites (CaO/Al_2O_3 < 1) rich in Al_2O_3 and CaO, the spectra of MORB-type rare earths have observed that they have undergone the effects of one or more partial melting processes of low degree and remained rather representative of a weakly depressed mantle. The protogranular textures

of lherzolites can also be interpreted more as the result of equilibration during reactions with a metasomatic agent during crystallization as well as the light rare earth enriched spectra of these rocks [51] [53]. This type of spectra is in fact compatible with a chromatographic effect due to the percolation of small fractions of basaltic liquids through peridotites initially depleted in light rare earths [52] [54] [55]. Fine-grained equigranular textures are formed in the most superficial levels of the lithospheric mantle, thanks to shear likely to connect the upper mantle and the upper crust [56]. The absence of dunites and garnet demonstrates that these xenoliths are compatible with a context of thinned and diapiric lithosphere in the superficial levels. Lithospheric upwellings may have started as early as the Triassic in the region, as evidenced by the presence of spinel lherzolites [57].

Conflicts of Interest

The authors declare no conflicts of interest regarding the publication of this paper.

References

[1] Déruelle, B., Ngounouno, I. and Demaiffe, D. (2007) The "Cameroon Hot Line" (CHL): A Unique Example of Active Alkaline Intraplate Structure in both Oceanic and Continental Lithospheres. *Comptes Rendus. Géoscience*, **339**, 589-600. https://doi.org/10.1016/j.crte.2007.07.007

[2] Kamgang, P. (2003) Pétrologie et géochimie d'un secteur clé de la Ligne du Cameroun, les monts Bamenda: Implications sur la genèse et l'évolution des magmas. Thèse Doct., University of Yaoundé I, Yaoundé, 373 p.

[3] Fitton, J.G. and Dunlop, H.M. (1985) The Cameroon Line, West Africa, and Its Bearing on the Origin of Oceanic and Continental Alkali Basalt. *Earth and Planetary Science Letters*, **72**, 23-38. https://doi.org/10.1016/0012-821X(85)90114-1

[4] Louis, P. (1970) Contribution géophysique à la connaissance géologique du bassin du lac Tchad. Mémoires OSTROM, n˚42, 311 p. et cartes en annexes.

[5] Browne, S.E. and Fairhead, J.D. (1983) Gravity Study of the Central African Rift System: A Model of Continental Disruption. Part 1: The Ngaoundéré and Abu Gabra Rifts. In: Morgan, P. and Baker, B.H., Eds., *Developments in Geotectonics*, Elsevier, Amsterdam, 187-203. https://doi.org/10.1016/B978-0-444-42198-2.50018-3

[6] Girod, M., Dautria, J.M. and Balle, S.D. (1984) Estimation de la profondeur du manteau du Moho sous le massif volcanique de l'Adamaoua (Cameroun) à partir de l'étude d'enclaves de lherzolite. *Comptes rendus de l'Académie des Sciences Paris* 2, **298**, 699-704.

[7] Stuart, G.W., Fairhead, J.D., Dorbath, L. and Dorbath, C. (1985) A Seismic Refraction Study of the Crustal Structure Associated with the Adamawa Plateau and Garoua Rift Cameroon, West Africa. *Geophysical Journal International*, **81**, 1-12. https://doi.org/10.1111/j.1365-246X.1985.tb01346.x

[8] Dautria, J.M. and Girod, M. (1986) Les enclaves de lherzolite à spinelle et plagioclase du volcan de Dibi (Adamaoua, Cameroun): Des témoins du manteau anormal. *Bulletin de Minéralogie*, **109**, 275-286. https://doi.org/10.3406/bulmi.1986.7934

[9] Poudjom Djomani, Y.P., Diament, M. and Albouy, Y. (1992) Mechanical Behaviour

of the Lithosphere beneath the ADAMAWA Uplift (Cameroon, West Africa) Based on Gravity Data. *Journal of African Earth Sciences*, **15**, 81-90. https://doi.org/10.1016/0899-5362(92)90009-2

[10] Dorbath, C., Dorbath, L., Fairhead, J.D. and Stuart, G.W. (1986) A Teleseismic Delay Time Study across the Central African Shear Zone in the Adamawa Region of Cameroon, West *Africa. Geophysical Journal International*, **86**, 751-766. https://doi.org/10.1111/j.1365-246X.1986.tb00658.x

[11] Thomas, P. (2004) Crustal Thinning and Associated Tectonic Subsidence during Continental Rifting. *Geophysical Journal International*, **158**, 529-553.

[12] Karmalkar, N.R., *et al.* (2002) Cryptic Metasomatism in the Upper Mantle beneath Kutch: Evidence from Spinel Lherzolite Xenoliths. *Current Science*, **82**, 1157-1165.

[13] Ngounouno, I., Déruelle, B. and Demaiffe, D. (2000) Petrology of the Bimodal Cenozoic Volcanism of the Kapsiki Plateau (Northern Most Cameroun, Central Africa). *Journal of Volcanology and Geothermal Research*, **102**, 21-44. https://doi.org/10.1016/S0377-0273(00)00180-3

[14] Tamen, J. (1998) Contribution à l'étude géologique du plateau Kapsiki (Extrême-Nord, Cameroun): Volcanologie, Pétrologie et Géochimie. Thèse Doct. 3ème cycle, Université de Yaoundé 1, Yaoundé, 127 p.

[15] Ngounouno, I. (1993) Pétrologie du magmatisme cénozoïque de la vallée de la Bénoué et du plateau Kapsiki (nord du Cameroun). Thèse Doct., Université Pierre et Marie Curie, Paris, 1-280.

[16] Dunlop, H.M. (1983) Strontium Isotope Geochemestry and Potassium-Argon Studies on Volcanic Rocks from the Cameroon Line, West Africa. PhD thesis, The University of Edinburgh, Edinburgh, 347.

[17] Vincent, P.M. and Armstrong, R.L. (1973) Volcanism of the Kapsiki Plateau (North Cameroon) and the Underlying Sedimentary Formations. Coll. African Geol., Florence.

[18] Okereke, C.S. (1988) Contrasting Modes of Rifting: The Benue Trough and the Cameroon Volcanic Line, West Africa. *Tectonophysics*, **7**, 775-784. https://doi.org/10.1029/TC007i004p00775

[19] Guiraud, R. and Maurin, J.C. (1992) Early Creataceous Rifts of Western and Central Africa: An Overview. *Tectonophysics*, **213**, 153-168. https://doi.org/10.1016/B978-0-444-89912-5.50035-1

[20] Moreau, C., Regnoult, J.M., Déruelle, B. and Robineau, B. (1987) A New Tectonic Model for the Cameroon Line, Central Africa. *Tectonophysics*, **139**, 317-334. https://doi.org/10.1016/0040-1951(87)90206-X

[21] Droop, G.T.R. (1987) A General Equation for Estimating Fe^{3+} Concentrations in Ferromagnesian Silicates and Oxides from Microprobre Analyses, Using Stoichiometric Criteria. *Mineralogical Magazine*, **51**, 431-435. https://doi.org/10.1180/minmag.1987.051.361.10

[22] Stormer, C.Fr. (1983) The Effects of Recalculation on Estimates of Temperature and Oxygen Fugacity from Analyses of Multicomponent Iron-Titanium Oxides. *American Mineralogist*, **68**, 586-594.

[23] Caldeira, R. and Munha, J.M. (2002) Petrology of Ultramafic Nodules from Sao Tomé Island, Cameroon Volcanic Line (Oceanic Sector). *Journal of African Earth Sciences*, **34**, 231-246. https://doi.org/10.1016/S0899-5362(02)00022-2

[24] Déruelle, B., Moreau, C., Nkoumbou Kambou, R., Lissom, J., Njonfang, E., Ghogomu, R.T. and Nono, A. (1991) The Cameroon Line: A Review. In: Kampuru,

A.B. and Lubala, R.T., Eds., *Magmatism in Extensional Structural Settings. The Phanerozoic African Plate*, Springer-Verlag, Berlin, 273-327. https://doi.org/10.1007/978-3-642-73966-8_12

[25] Lee, D.C., Halliday, A.N., Davies, G.R., Essene, E.J., Fitton, G.J. and Temdjim, R. (1996) Melt Enrichment of Shallow Depleted Mantle: A Detailed Petrological, Trace Element and Isotopic Study of Mantle-Derived Xenoliths and Megacrysts from the Cameroon Line. *Journal of Petrology*, **37**, 415-441. https://doi.org/10.1093/petrology/37.2.415

[26] Nana, R., Nkoumbou, C., Tchouankoué, J.P., Tabod, F. and Tchoua, F. (1998) Pétrologie des nodules de péridotites de Nyos (Cameroun): Implications sur l'évaluation des risques volcaniques. In: Vicat, J.-P. and Bilong, P., Eds., *Géosciences au Cameroun*, Press. Univ., Yaoundé I, Yaoundé, 225-228.

[27] Princivalle, F., Tirone, M. and Comin-Chiaramonti, P. (2000) Clinopyroxenes from Metasomatized Spinel-Peridotite Mantle Xenoliths from Nemby (Paraguay): Crystal Chemistry and Petrological Implications. *Mineralogy and Petrology*, **70**, 25-35. https://doi.org/10.1007/s007100070011

[28] Nkouandou, O.F. and Temdjim, R. (2011) Petrology of Spinel Lherzolite Xenoliths and Host Basaltic Lava from Ngao Voglar Volcano, Adamawa Massif (Cameroon Volcanic Line, West Africa): Equilibrium Conditions and Mantle Characteristics. *Journal of Geosciences*, **56**, 375-387. https://doi.org/10.3190/jgeosci.108

[29] Morimoto, N., Fabries, J., Ferguson, A.K., Ginzburg, I.V., Ross, M., Seifert, F.A., Zussman, J., Aoki, K. and Gottardi, G. (1988) Nomenclature of Pyroxenes. *American Mineralogist*, **73**, 1123-1133.

[30] Simkim, T. and Smith, J.V. (1970) Minor Element Distribution in Olivine. *The Journal of Geology*, **78**, 207-219. https://doi.org/10.1086/627519

[31] Roeder, P.L. and Emslie, R.F. (1970) Olivine-Liquid Equilibrium. *Contributions to Mineralogy and Petrology*, **29**, 275-508. https://doi.org/10.1007/BF00371276

[32] Vaselli, O., Downes, H., Thirwall, M., Dobosi, G., Coradossi, N., Seghedi, I., Szakacs, A. and Vannucci, R. (1995) Ultramafic Xenoliths in Plio-Pleistocene Alkali Basalts from the Eastern Transylvanian Basin: Depleted Mantle Enriched by Vein Metassomatism. *Journal of Petrology*, **36**, 23-53. https://doi.org/10.1093/petrology/36.1.23

[33] Sun, S.S. and McDonough, W.F. (1989) Chemical and Isotopic Systematics of Oceanic Basalts: Implications for Mantle Composition and Processes. In: Saunders, A.D. and Norry, M.J., Eds., *Magmatism in the Ocean Basins*, Vol. 42, The Geological Society, London, 313-345. https://doi.org/10.1144/GSL.SP.1989.042.01.19

[34] Ngounouno, I. and Déruelle, B. (2007) Pétrologie des xénolites de wehrlites et clinopyroxénites du mont Cameroun: Évidence d'un métasomatisme mantellique. *Journal of the Cameroon Academy of Sciences*, **7**, 35-46.

[35] Matsui, Y. and Nishizawa, O. (1974) Iron (II)-Magnesium Exchange Equilibrium between Olivine and Calcium-Free over a Temperature Range 800 ˚C to 1300 ˚C. *Bulletin de Minéralogie*, **97**, 122-130. https://doi.org/10.3406/bulmi.1974.6868

[36] Ganguly, J. and Ghose S. (1979) Aluminous Orthopyroxene: Order-Disorder, Thermodynamic Properties and Petrologic Implications. *Contributions to Mineralogy and Petrology*, **69**, 375-385. https://doi.org/10.1007/BF00372263

[37] Ben Jamma, N. (1988) Les péridotites de Bay of Islands (Terre Neuve) et de Cap Ortegal (Espagne): Approche petro-structurale. Thèse de Doctorat, I.P.G.P. & Univ. Paris 7, Paris, 245 p.

[38] Bertrand, P., Sotin, C., Gaulier, J.M. and Mercier, J.C.C. (1987) La solubilité de

l'aluminium dans l'orthopyroxène. Inversion globale des données expérimentales de MgO-Al_2O_3-SiO_2. *Bulletin de la Société Géologique de France*, **3**, 821-832. https://doi.org/10.2113/gssgfbull.III.5.821

[39] Mercier, J.C. (1980) Magnitude of Continental Lithospheric Stresses Inferred from Rheomorphic Petrology. *Journal of Geophysical Research*, **85**, 6293-6303. https://doi.org/10.1029/JB085iB11p06293

[40] Webb, S.A. and Wood, B.J. (1986) Spinel-Pyroxene-Garnet Relationships and Their Dependance on Cr/Al Ratio. *Contributions to Mineralogy and Petrology*, **92**, 471-480. https://doi.org/10.1007/BF00374429

[41] Cabanes, N. and Mercier, J.C.C. (1988) Insight into the Upper Mantle beneath an Active Extensional Zone: The Spinel-Peridotite Xenoliths from San Quintin (Baja California, Mexico). *Contributions to Mineralogy and Petrology*, **100**, 374-382. https://doi.org/10.1007/BF00379746

[42] Benoit, V. (1987) Etat d'équilibre de péridotites du manteau supérieur: Application du plateau du Colorado. Ph.D. Thesis, Université Paris 7, Institut Physique du Globe de Paris, Paris.

[43] Fabriès, J. (1979) Spinel-Olivine Geothermometry in Peridotite from Ultramafic Complexes. *Contributions to Mineralogy and Petrology*, **69**, 329-336. https://doi.org/10.1007/BF00372258

[44] Green, D.H. and Hibberson, W. (1970) The Instability of Plagioclase in Peridotite at High Pressure. *Lithos*, **3**, 209-221. https://doi.org/10.1016/0024-4937(70)90074-5

[45] Adams, G.E. and Bishop, F.C. (1986) The Olvine-Clinopyroxene Geobarometer: Experimental Results in the CaO-FeO-MgO-SiO_2 System. *Contributions to Mineralogy and Petrology*, **94**, 230-237. https://doi.org/10.1007/BF00592939

[46] Nimis (1998) Clinopyroxene Geobarometry of Magmatic Rocks Part 1: An Expanded Structural Geobarometer for Anhydrous and Hydrous, Basic and Ultrabasic Systems. *Contributions to Mineralogy and Petrology*, **133**, 122-135. https://doi.org/10.1007/s004100050442

[47] Carswell, D.A., Griffin, W.L. and Kresten, P. (1984) Peridotite Nodules from the Ngopetsoen and Lipelaneng Kimberlites, Lesotho: A Crustal or Mantle Origin. In: Kornprobst, J., Ed., *Kimberlites II: The Mantle and Crust-Mantle Relationships*, Elsevier, Amsterdam, 229-243. https://doi.org/10.1016/B978-0-444-42274-3.50025-1

[48] Fabriès, J., Lorand, J.-P., Bodinier, J.-L. and Dupuy, C. (1991) Evolution of the Upper Mantle beneath the Pyrenees: Evidence from Orogenic Spinel Lherzolite Massifs. *Journal of Petrology*, No. 2, 55-76. https://doi.org/10.1093/petrology/Special_Volume.2.55

[49] Nicolas, A., Lucazeau, F. and Bayer, R. (1987) Peridotite Xenoliths in Massif Central Basalts, France: Texture and Geophysical Evidence for Asthenospheric Diapirism. In: Nixon, P.H., Ed., *Mantle Xenoliths*, John Wiley and Sons, Chichester, 563-574.

[50] Bodinier, J.-L., Menzies, M.-A. and Thirlwall, M.-F. (1991) Continental to Oceanic Mantle Transition-REE and Sr-Nd Isotopic Geochemistry of the Lanzo Lherzolite Massif. *Journal of Petrology*, No. 2, 191-210. https://doi.org/10.1093/petrology/Special_Volume.2.191

[51] Frey, F.A., Suen, J. and Stockman, H.W. (1985) The Ronda High Temperature Peridotite Geochemistry and Petrogenesis. *Geochimica et Cosmochimica Acta*, **49**, 2469-2491. https://doi.org/10.1016/0016-7037(85)90247-9

[52] Bussod, G.-Y. and Christie, J.-M. (1991) Textural Development and Melt Topology in Spinel Lherzolite Experimentally Deformed at Hypersolidus Conditions. *Journal of Petrology*, No. 2, 17-40. https://doi.org/10.1093/petrology/Special_Volume.2.17

[53] Mysen, B.O. and Kushiro, I. (1977) Compositional Variations of Coexisting Phases with Degree of Partial Melting of Peridotite in the Upper Mantle. *American Mineralogist*, **62**, 843-865.

[54] Navon, O. and Stolper, E. (1987) Geochemical Consequence of Melt Percolation: The Upper Mantle as a Chromatogaphic Column. *The Journal of Geology*, **95**, 285-307. https://doi.org/10.1086/629131

[55] Fabriès, J., Lorand, J.-P. and Bodinier, J.-L. (1998) Petrogenetic Evolution of Orogenic Lherzolite Massifs in the Central and Western Pyrenees. *Tectonophysics*, **292**, 145-167. https://doi.org/10.1016/S0040-1951(98)00055-9

[56] Midoun, M. and Perthuisot, V. (1992) Les éléments de socle inclus dans les évaporites du Trias (région d'Oran, Algérie) Implications sur les caractéristiques du substratum et sur l'amincissement lithosphérique triasique. *Comptes rendus de l'Académie des Sciences Paris*, *série* II, **315**, 571-577.

[57] Teitchou, M., Gregoire, M., Dantas, C. and Tchoua, F.M. (2007) Le manteau supérieur à l'aplomb de la Plaine de Kumba (Ligne du Cameroun), d'après les enclaves de péridotites à spinelles dans les laves basaltiques. *Comptes Rendus. Géoscience*, **339**, 101-109. https://doi.org/10.1016/j.crte.2006.12.006